Active-Adaptive Control of Inlet Separation Using Supersonic Microjets

Final Report
NASA Grant Number: NAG-1-02059

Prepared by
F. S. Alvi

Farrukh S. Alvi
Principal Investigator, Associate Professor,
The Department of Mechanical Engineering
FAMU-FSU College of Engineering
Florida A & M University
Tallahassee, FL 32310

Executive' Summary

Flow separation in internal and external flows generally results in a significant degradation in aircraft performance. For internal flows, such as inlets and transmission ducts in aircraft propulsion systems, separation is undesirable as it reduces the overall system performance. The aim of this research has been to understand the nature of separation and more importantly, to explore techniques to actively control it. In this research, we extended our investigation of active separation control (under a previous NASA grant) where we explored the use of microjets for the control of boundary layer separation. The geometry used for the initial study was a simple diverging 'Stratford' ramp, equipped with arrays of microjets. These early results clearly show that the activation of microjets eliminated flow separation. Furthermore, the velocity-field measurements, using PIV, also demonstrate that the gain in momentum due to the elimination of separation is at least an order of magnitude larger (two orders of magnitude larger in most cases) than the momentum injected by the microjets and is accomplished with very little mass flow through the microjets.

Based on our initial promising results this research was continued under the present grant, using a more flexible model. This model allows for the magnitude and extent of separation as well as the microjet parameters to be independently varied. The results, using this model were even more encouraging and demonstrated that microjet control completely eliminated significant regions of flow separation over a wide range of conditions with almost negligible mass flow. Detailed studies of the flowfield and its response to microjets were further examined using 3-component PIV and unsteady pressure measurements, among others. As the results presented this report will show, microjets were successfully used to control the separation of a much larger extent and magnitude than demonstrated in our earlier experiments. In fact, using the appropriate combination of control parameters (microjet, location, angle and pressure) separation was completely eliminated for the largest separated flowfield we could generate with the present model.

Separation control also resulted in a significant reduction in the unsteady pressures in the flow where the unsteady pressure field was found to be directly responsive to the state of the flow above the surface. Hence, our study indicates that the unsteady pressure signature is a strong candidate for a 'flow state sensor', which can be used to estimate the location, magnitude and other properties of the separated flowfield. Once better understood and properly utilized, this behavior can be of significant practical importance for developing and implementing online control.

1. Introduction

The separation of boundary layers is generally undesirable in most applications due to the many related adverse effects, such as increased flow unsteadiness, pressure losses, and the increase in drag. An area where prevention of flow separation may yield significant dividends in terms of improved efficiency are engine inlets and diffuser ducts. Most conventional solutions for separation prevention or control, such as increasing the inlet length, are generally not practical due to penalties imposed by such 'solutions'. For example, increasing the inlet length may increase the size of the overall vehicle[1] thus increasing drag and aircraft weight. In addition, for certain military applications, a serpentine inlet is used to block the line of sight[2, 3] to the compressor face, thereby reducing the radar signature from the compressor face.

Similar "buried" propulsion systems have also been considered for the Blended Wing Body (BWB) design[4]. Flow distortion and separation is especially an area of concern for such designs where engines are located at the aft end of the aircraft. This requires the ingestion of a thick and generally degraded boundary layer that is more susceptible to separation due to adverse pressure gradients encountered in the duct. Not only is the pressure loss undesirable, the distortion and unsteadiness created due to the separated flow can also result in aerodynamic stall and surge in the compressor and fan blades[5, 6]. Consequently, it is highly desirable to avoid boundary layer separation in inlets as it can lead to significant reductions in the engine performance.

Numerous approaches for controlling boundary layer separation have been explored[7, 8]. These include: a) Tangential blowing to directly energize the incipiently separating or separated boundary-layer[9-11], b) Wall suction[12,13] c) Vortex generators (v.g's and micro v.g.'s) in the form of vanes and 'bumps'[14,15] and d) Forced excitation devices e.g. acoustic excitation[16,17] and synthetic jets[18,19]. Although the active control methods, suction and tangential blowing, have been somewhat successful, the associated cost in terms of mass flux, make them impractical. Vortex generators have been widely examined for separation control, where v.g.'s of various shapes and sizes have been explored[15]. Although the mechanism is still not well understood, it has been suggested that the v.g.'s produce strong vortices, which enhance the mixing between the high momentum core flow and the low momentum boundary layer flow, thus energizing the boundary layer fluid[1]. However, the performance of these v.g.'s, which are passive in nature, has been somewhat limited; usually there is a need to optimize their location, size and other parameters to achieve optimal performance for specific operating conditions. In addition, they have an associated parasitic drag when they are not in use.

As discussed in the review article by Greenblatt and Wygnanski[20] the use of acoustic excitation methods for separation control (over airfoils), certain methods, such as those used by Ahuja et. al[17] and Zaman et. al[16] have shown some benefits. However, these acoustic excitation studies were in most cases facility dependant and therefore of limited use from a practical perspective. Synthetic jets[18] are another popular active flow method which have also been examined for separation control applications. Amitay et al.[18] demonstrate that their synthetic jet-based actuators provided some control of flow separation in a duct. The measurements of Amitay et al consisted of pitot surveys which showed that flow attachment was generally obtained for a limited region of the flowfield and complete reattachment was limited to a few cases. Similar synthetic jets were used by Jenkins et al[19] for controlling flow separation over an adverse pressure gradient ramp (almost identical to one of the model used in the present research). Jenkins et al. conclude that the synthetic jets did not work, primarily due to "insufficient velocity/momentum output" which is essential to achieve effective control.

In this research, we explore a different and novel approach that uses high-momentum, low mass flux, microjets to control flow separation. Based on their success in other applications[21] and the low mass flow rates required, we anticipated that these active flow control devices may also be effective for separation control. Jets in crossflow, which in essence is the flow generated by the microjet actuators, generate longitudinal (streamwise) vortices[22] upon interaction with a boundary layer. These vortices energize the near-wall fluid by promoting mixing with the outer fluid. We anticipate that that microjets would thus act as efficient fluidic vortex generators, energizing the boundary layer fluid by creating strong streamwise vorticity[23] thereby enhancing mixing with the more energetic flow. Furthermore, due to their small size, simplicity and ease of implementation, this approach, if successful, can in principal be relatively easily implemented in engine inlet ducts or other applications, such as airfoils.

The study described here is a continuation of the work that was initiated under a prior NASA grant, whose promising results prompted us to further develop and explore the present control approach. In addition to the support from NASA, the Air Force Research Laboratory (AFRL) also funded a small portion of our separation control research through a 1-year grant. Since the three research efforts are intimately connected; for the sake of completeness and to put the results in their proper context, the results described herein include some obtained under the other grants.

2. Experimental Details: Hardware and Methods

The experiments were conducted in a subsonic, closed return, wind tunnel with a maximum freestream velocity of 65m/s in the 48"x24" test section. The initial test model used consisted of an adverse pressure gradient ramp, similar to model used at the NASA Langley Research Center for examining the effectiveness of various control techniques[19]. This geometry produces a Stratford like pressure gradient[24] in the test section. A picture of this earlier model, mounted in the wind tunnel, is shown in Fig. 1. In the latter part of this research a more complex model, shown in Fig. 11 and described in §5 was used.

A schematic of this first ramp model, subsequently referred to as the 'fixed' ramp is also shown in Fig. 2, where the ramp begins at X=0″ and is preceded by a flat region of 21.5″. The figure also shows the region where PIV measurements were obtained — at two longitudinal planes, along the centerline and 0.1S away form the centerline, where S is the span of the ramp. This off-centerline plane is referred to as the "0.4S" location. Also, shown in the figure are the locations of microjets, only the 1st and 3rd array of microjets were used for control purposes on this model. Each row consists of about 60 microjets, 400μm in diameter. The microjets were oriented vertically, i.e. 90° with respect to the free-stream. The placement of these microjets with respect to separation location was expected to be a critical parameter for the control scheme. It was anticipated that the actuators should be placed upstream of the separation zone for optimal effect. Since the exact location of the separation was not known a priori, the microjets were placed upstream of the region where separation was observed in the NASA study[19]. The microjets were supplied with nitrogen from compressed gas tanks since N_2 is easily available in pure form and has essentially the same gas dynamic properties as air.

In addition to the conventional mean surface pressures, the unsteady surface flow properties were examined through unsteady surface pressure measurements using Endevco® (Model 8510B-1) pressure transducers. More details regarding the unsteady pressure hardware and the results are presented in §6.2. The flowfield above the surface was explored using the two-component (2-D) and 3-component Particle Image Velocimetry (PIV) techniques. Two-component measurements were obtained in longitudinal/streamwise planes for the fixed ramp, while both two and three-component measurements were obtained for the next-generation model. The fixed- model PIV results are discussed in §3.2 while the result for the new model are in §6.2 and 6.4

3. Results: Fixed Ramp Model

The results obtained with the first, fixed ramp model, are very briefly discussed here in order to provide the context for the more recent results which are discussed in detail in section §6. More details on these can be found in Kumar and Alvi [25]. Experiments were conducted over an extended range of freestream velocities of 10m/s - 65m/s, using various combinations of microjet locations and pressures. In this section, unless otherwise stated, only results for 40m/s are discussed as this case illustrates the principal flow features and its response to microjet control. The Reynolds number at the ramp leading edge at U_∞=40m/s is 1.26×10^6. At this velocity, the boundary layer thickness, δ, measured at the leading edge at the centerline (using a boundary layer pitot probe) was found to be 0.75 inches. The boundary-layer profile was in close agreement with seventh power law profile indicating that the incoming boundary layer is nominally turbulent. The corresponding displacement thickness, δ^* and the momentum thickness, θ at the ramp leading edge were estimated to be 0.12″ and 0.08″, respectively.

3.1 Surface Flowfield Visualization

The surface flow field was visualized to identify the principal flow features, especially the extent of the separation region. The surface streamline pattern for flow without control is shown in Fig. 3a. Also drawn on Fig. 3a, are the streamlines indicating the flow direction. These streamlines have been drawn based on the visual observations during the experiment. The horizontal streamlines in the upstream, left half, of Fig. 3a indicate that the flow field is uniform and nominally two-dimensional. In contrast, significant three-dimensional effects can be observed immediately downstream of the ramp leading edge. A 'secondary flow' near the ramp edges also (see Fig. 3a) appears just downstream of the location where the ramp begins. This secondary flow may in part be due to corner vortices generated at the edges of the model.

The surface flow essentially shows a 'trapped' separation bubble, generated due to the adverse pressure gradient. The effect of flow control on the surface flow pattern is shown in Fig. 3b where no regions of reverse velocity are visible once microjets are activated. The flow pattern, however, is not completely two-dimensional and three-dimensional features, such as diverging streamlines, can be noticed. As discussed later, it is anticipated that one of the mechanism at work in the present control technique is the introduction of streamwise vorticity by the microjets. As such, one may argue that some of the features in Fig. 3b are similar to footprints of streamwise vortices. However, based on surface flow visualizations alone, the exact

nature of these features can not be deciphered. What is clear is that the microjets eliminate the large 3D separation bubble seen in Fig. 3a. To further understand the nature of the base flow and its response to microjet control, more detailed measurements, especially velocity field measurements using PIV were obtained; these are discussed in the next and later sections.

3.2 Velocity/Vorticity Field Measurements

The velocity field above the surface was explored in detail using the two-component, (sometimes also referred to as 2-D) Particle Image Velocimetry (PIV) technique for the fixed ramp. For this case, PIV measurements were obtained along the centerline plane and at two planes off-centerline, as described in §2. Only velocity-field data for the 'Centerline' plane (see Fig. 2b) has been presented here for the sake of brevity. The test section was seeded with smoke particles, using a Rosco fog generator and was illuminated using a New Wave[TM] Nd-YAG pulsed laser with a repetition rate of 15Hz. The images were acquired using a Kodak ES 1.0 high-resolution CCD camera capable of recording 10-bit digital image pairs in separate frames at a rate of 15-image pairs/second. Further details of this PIV technique can be found in Lourenco[28] and Lourenco et al.[29]

3.2.1 Baseline (No Control) Case:

An example of a typical instantaneous velocity vector field for the no control case is shown in Fig. 4a. As seen here, a significant reverse flow region is clearly evident. A discussion of the flowfield with microjets activated, shown in Fig. 4b, is delayed until the effect of control is discussed later in this report. For a better understanding of the separated flowfield and the effect of microjet control, the mean flow properties are discussed next. We begin with Fig. 5a which shows the streamwise component U, of the mean velocity field in the centerline plane, for a freestream velocity of 40m/s. Unless otherwise stated, in this and all subsequent 2D-PIV data discussed in this report, the ramp model is on the top of the plot from which the microjets issue vertically down; freestream flow is from left to right. The inset in Fig. 5a shows the ramp geometry and the region where the PIV data was obtained. All the distances are non-dimensionalized with respect to the ramp height and the y-axis represents the vertical distance from the base of the ramp and the x-axis is the streamwise distance from the ramp leading edge (see Fig. 2a for coordinate frame).

A closer examination of Fig. 5a shows that as one proceeds downstream in the vicinity of the surface, there is a rapid deceleration in the fluid velocity, which eventually leads to a region

of reverse flow. This reverse flow zone corresponds to the dark blue velocity contours (Fig. 5a) and starts around x/H = 1.6 approximately ending around x/H = 2.2. A small sub-region of this flow field, roughly indicated by the box in Fig. 5a, has been magnified in Fig. 5b, where the presence of reverse flow, close to the ramp surface, is clearly visible confirming that the flow has separated locally resulting in a separation bubble. Contour plots of the vertical component of velocity (not shown here) clearly reveal the presence of low magnitude velocity fluid moving away from the boundary in the same region where reverse flow field is seen in Fig. 5. As noted in §3.1, this separation appears to be three-dimensional in nature. Hence, 2-component PIV measurements were obtained at three off-centerline axial planes to provide some insight into the three-dimensional effects. Although not shown here, a comparison to the centerline velocity field (Fig. 5a) reveals that as one moves away from the centerline plane, the size of the bubble at grows appreciably larger (at the 0.4W plane) and then reduces as one approach the sides of the ramp. This result is consistent with our earlier observation based on the surface flow pattern.

3.2.2 Effect of Microjet Control

The effect of microjets can be clearly seen from the instantaneous velocity vector field in Fig. 4b. This flow was generated with the activation of the 3rd array of microjets, MJ3, operating at 25psig. A comparison with Fig. 4a clearly illustrates that not only has the reverse velocity zone been eliminated, but, there has also been a significant momentum addition along the surface. To study this effect of microjets, the influence of various parameters on separation control was examined, as described next.

The first parameter considered was the freestream velocity. Fig. 6a presents the mean streamwise velocity data for the centerline plane at 40m/s, where the 3rd array of microjets is operating at 25psig. A comparison of Fig. 6a with Fig. 5a shows that the activation of microjets completely eliminates the reverse flow region; very similar effects were also observed for the 50m/s case (not shown), where the separated flowfield was 15-20 % larger. Furthermore, for U_∞ = 40m/s, the velocity near the surface with microjet control was higher than for the 50m/s case. This intuitively suggests that the ratio of the microjet momentum relative to the freestream momentum may be a relevant parameter, requiring further study. Of course, the influence of momentum flux ratio is well known and has been discussed by numerous others[20].

Steady Momentum Flux Ratio

To better understand and quantify the efficacy of microjet control in terms of the mass and momentum flux supplied by the microjets, these parameters were further explored, as described next. Here, the mass flux coefficient, M^*, and the steady momentum coefficient, C_μ were defined as follows:

M^* = (Mass flux of the microjets) / (Mass deficit based on δ)

where, δ is the boundary layer thickness at the ramp leading edge.

The mass flow rate, m_{in}, through the microjets can be conservatively estimated by assuming choked flow through the micro-nozzles. The mass coefficient is then given as:

$$M^* = \frac{m_{in}}{\rho_\infty U_\infty y \delta}$$

where, ρ_∞ is the freestream density, U_∞ is the freestream velocity, and y is the span of the ramp.

The momentum flux ratio is given by the conventional definition of the steady momentum coefficient[20] and is given as

$$C_\mu = \frac{N m_{in} U_j}{\frac{1}{2}\rho_\infty U_\infty^2 y \delta}$$

where N is the number of microjets, and U_j is the jet velocity.

Thus, C_μ is the ratio of the magnitude of the total momentum injected into the flow relative to the freestream dynamic pressure multiplied by an appropriate area – chosen as δy in the present case. These values of C_μ and M^* for various microjet operating pressures have been plotted in Fig. 7. As expected, C_μ and M^* are related such that small increments in M^* yield progressively larger C_μs, thus accounting for the effectiveness of microjets with relatively little mass flow injection. Measurements show that increasing the microjet operation pressures, i.e. increasing the C_μ , results in higher velocities closer to the ramp surface, indicating the presence of higher momentum in the near-wall region. The reason behind this behavior may be due to one or more of the following; as C_μ increases: a) more momentum is directly injected into the boundary layer, b) strong streamwise vortices[22] are generated which enhance mixing with the outer, high momentum fluid and or c) The microjet jet momentum and penetration depth[30, 31] increases, enhancing the transfer of momentum from the freestream fluid to boundary layer fluid.

A magnified view of a selected region for the 40m/s case (Fig. 6a) is shown in Fig. 6b. Upon a comparison with the corresponding baseline case, Fig. 5b, it is clear that the activation of microjets has led to the addition of significant momentum in the forward direction in the zone

previously corresponding to reverse flow. At 25 psig, the mass flux supplied by the microjets is approximately 1.7 % of the mass flux across the ramp, based on the boundary layer thickness, i.e. M* = 0.017. This pressure corresponds to a C_μ of 0.397 or 39.7%, which amounts to a C_μ of 6.3e-03/jet, significantly higher than the 2e-03/jet values quoted using synthetic jets [18].

The second parameter examined in terms of microjet efficiency is the location of the actuators. In general, it is well-accepted that a separation control input must be applied at or close to the separation point. Hence, experiments were conducted with microjets at different axial locations along the ramp where all the microjet arrays were successful in eliminating the reverse flow region *regardless of their location*. However, upon comparing the effect of MJ1 (shown in Fig. 6a) with that of the 3rd array, MJ3, it appears that, although separation is eliminated for both, measurably higher velocities, and closer to the surface, were obtained with the activation of MJ3. In addition, the reverse flow region was eliminated with a lower momentum flux input using MJ3 compared to MJ1. This reinforces the fact that choosing the appropriate location for applying flow control is a very important consideration.

Whether the microjets eliminate the entire three-dimensional separation region was also examined using the PIV results acquired at the Off-Centerline locations. Separation was eliminated everywhere, although the effect of control was not as pronounced in the off-centerline planes. For example, the magnitude of the streamwise component of the velocity was somewhat lower for the off-centerline cases relative to the velocities measured along the centerline. This may in part be due to the three dimensional nature of the separation bubble and perhaps also due to the presence of secondary corner flow, which was previously discussed. Although the details of the effect of microjets on the entire three-dimensional flow are not completely understood at present, there is no doubt that overall, microjets eliminate or significantly reduce the size of the separation region. Further study of the three-dimensional effects is warranted.

4. The Effect of Microjets on the Boundary Layer Momentum

One may ask whether the significant increase in the momentum near the ramp surface is simply due to the direct injection of momentum by the microjets or some other mechanism(s). To gain some insight into this we examine our results in terms of the mass and momentum flux through the microjets. We begin with defining a parameter, referred to as the '*momentum gain ratio*', **MGR**, which is the ratio of the increase in momentum due to microjet control relative to the momentum injected by the microjets. Hence, MGR is given as:

$$MGR = \frac{momentum_{With\ Control} - momentum_{No\ Control}}{momentum_{microjets}}$$

$$= \frac{\int (\rho U dA)_{With\ Control} - \int (\rho U dA)_{No\ Control}}{N\dot{m}_{in} U_j}$$

The momentum flux with and without control was calculated at axial locations by numerically integrating the velocity field data. A comparison of the momentum gain achieved with the application of different microjets at various operating pressures is listed in Table 1 and a corresponding plot is shown in Fig. 8. Both the tabulated results and the plot clearly show that for the same C_μ values the momentum gain achieved with MJ3 is significantly more than that achieved with MJ1. In particular, at 25psig, the momentum gain with MJ1 is 7.8, while the momentum gain achieved with MJ3 is 30. This reaffirms the notion that the location of the actuators relative to the separation location plays a very important role in the efficacy of control. It also strongly suggests that closer one is to the separation location; more effective control can be achieved.

This high momentum gain ratio clearly indicates that some other mechanism(s), *distinct from direct injection of momentum* plays an important role in this control approach. As mentioned earlier, one of the physical mechanisms we expect to be of significance is the generation of streamwise vorticity by the microjets[22, 32]. This streamwise vorticity is expected to enhance the entrainment of the freestream fluid into the boundary layer. In addition, it may also promote mixing between the low momentum portions of the boundary layer, very close to the surface, with the higher momentum fluid away from the wall, thus preventing or delaying separation.

To explore this further, we sought to delineate the effects of flow control on the momentum gain (MGR) into two regions as follows. We first identify a region where the near-wall fluid 'directly' encounters the microjets and define its extent as the maximum penetration depth of the microjets. Hence, this defines the zone in which the microjets may influence the local flow directly. The second zone is the remainder of the boundary layer flow outside the area of direct influence. In this second zone, the gain in momentum due to flow control may be more strongly influenced by other mechanisms, such as the generation of streamwise vorticity, physical mechanisms that we collectively refer to as the 'secondary effects' of the microjets. As documented by others[22, 33], the penetration depth of jets in cross-flow is mainly a function of the momentum ratio. Although there are a number of primarily empirical correlations available in

literature for estimating the penetration of jets in cross-flow, for the present analysis, the maximum jet penetration, Y_{max} of a single jet into a duct with a cross-flow was evaluated using Norster's equation[30].

$$\frac{Y_{max}}{d_j} = 1.15 \times \left(\frac{\rho_j U_j^2}{\rho_\infty U_\infty^2} \right)^{0.5} \times \sin(\delta_j)$$

where ρ_j is the jet density, d_j is the jet diameter and δ_j is the microjet blowing angle at the *vena contracta*.

Using the above correlation, the penetration of the microjets was determined to be approximately 0.2″, almost 1/4th of the boundary layer thickness. This leads to the definition of the region of direct influence as that below this 'quarter' boundary layer plane, $\delta_{0.25}$. Outside $\delta_{0.25}$, one would expect the gain in momentum to be due to the secondary effects, as discussed above. Using these definitions, the momentum again ratio for MJ3 operating at 25psig is evaluated at various axial locations for both the direct and secondary effects and the results are shown in Fig. 9. The plot shows that downstream of the microjet injection location, the 'direct effect' initially starts to grow rapidly. This initial rapid growth of the direct effect zone occurs in the vicinity of the microjet injection location, a region generally identified as where the initial evolution – penetration into and turning due to the freestream flow – occurs[34, 35]. Further downstream, the momentum gain due to the direct effects appears to saturate and even decline. However, the contribution of the secondary effects continues to grow downstream of the injection location and plays a proportionally larger role as one move downstream. This suggests that the secondary effects - which we suspect to be due to the generation of streamwise vorticity – continue to energize the boundary layer flow by entraining high momentum fluid from the freestream. There are a number of approaches one can use to examine the results obtained in our study to better elucidate the flow physics behind this control technique; the preceding analysis and discussion is a one simple, phenomenological-based, attempt to do so. However, what it clearly demonstrates is that the present control technique is not effective simply due to the direct injection of momentum into the boundary layer of fluid. If such were the case, the mass flow requirement to achieve separation and distortion control would make this approach impractical.

Next, we briefly study the effect of microjets on flow unsteadiness. Fig. 10a and 10b present the fluctuating component of the streamwise velocity, U_{rms} for the uncontrolled and the controlled cases, respectively for principal test case (40m/s, MJ3 activated at 25psig for the controlled case). In these contour plots, U_{rms} has been non-dimensionalized with the freestream

velocity. A comparison of Fig. 10a with Fig. 10b, illustrates that the velocity fluctuations associated with the flow have been dramatically reduced, by as much as 50% or more. In fact, most of the regions associated with high fluctuations have disappeared. Not only have the velocity fluctuations have been reduced in magnitude, but also the regions in which these fluctuations occur have become much smaller. Although not shown here, a comparison of turbulence kinetic energy associated with the uncontrolled and controlled cases was also made[25]. It was observed that level of turbulence associated with the flow was also reduced by almost 50%; similar effects were observed at higher freestream velocities.

To summarize, although the physical mechanisms behind microjet control still need to be explored further, based on the use of microjets in other applications[21, 23, 32] and the preceding results, it appears that the streamwise vorticity due to the microjets may play a primary role in this control approach. The generation of streamwise vorticity can be due to a number of mechanisms. First, the microjets may behave as fluidic 'tabs' much like the micro-v.g.'s used in earlier work[14,15,19]. Second, the vorticity in the microjets is redirected in the streamwise direction by the mean flow, and finally the microjets may also redirect the spanwise vorticity in the base flow in the streamwise direction by vorticity 'tilting'. These mechanisms may be similar to those discussed by Alvi et al.[32] in the context of impinging jet control using microjets. Direct evidence of the role of vorticity is presented in section 6.

5. Microjets Explored Further- Details of the New Model

In this section, we will discuss our study of microjet separation control using the next generation, more flexible ramp model. Based on the lessons learned from our initial study with the fixed model (which was used for approx., the first half of the research under the present NASA grant) a more flexible geometry both in the terms of the severity of separation and the microjet control parameters was needed. Some parameters that are expected to have a significant effect on the separation location, size and the control mechanism are as follows:

- o   Nature of pressure gradient, dp/dx (i.e. ramp geometry)
- o   Reynolds number, Re
- o   Location of microjets w.r.t. separation location
- o   The relative momentum supplied, by the microjets, referred to as the momentum coefficient, C_μ.
- o   Angle at which momentum is supplied to the boundary layer
- o   Angle of attack of the ramp, θ.
- o   Spacing between the microjets.

To explore these parameters in a more detailed manner and to concomitantly obtain a better understanding of the physical mechanisms responsible for the effectiveness of microjet control, a new model was designed and fabricated. The new model is highly flexible in that is allows the base flow as well as the control parameters to be varied. For example, the ramp can be rotated about a pivot point which changes the adverse pressure gradient experienced by the flow, thereby controlling the nature – size and location – of the separated flow.

This model has almost 30 static pressure taps along the centerline and more than 60 taps in the transverse direction at strategic locations. A picture of this Aluminum model is shown in Fig. 11a. The model also incorporates 7 arrays of microjets through an actuator insert, shown in Fig. 11b. The microjets are 400μm in diameter with spacing of 5mm and are located strategically around the separation location, keeping in mind that the separation location changes with ramp angle of attack. This microjet insert has slots for microjet modules, which are shown in Fig. 11d. Each modules has arrays of microjets oriented at various angles and the modules are interchangeable, i.e. they can be inserted in any of the seven slots. A magnified view of the module revealing microjets is also shown in Fig. 11d. The locations of these microjets and the modular insert are also shown in Fig. 12a and Fig. 12b. These flexibilities in the ramp model allowed us to study the parametrical effects on separation location in much detail.

6. Results: Using the New Ramp Model
6.1 Two-Component PIV Measurements
6.1.1 Baseline Case

Quantitative velocity field data was first obtained using 2D-PIV along the centerline plane of the new model. The location of these PIV measurements is shown in Fig. 12a and 12b.A representative of the ensemble averaged velocity field for a freestream velocity of 40m/s has been shown in Fig. 13 where the ramp is at an angle of 5° (see Fig. 12b) and flow is from left to right. In these plots, length scales are non-dimensionalized with respect to ramp height, H. (Note that increasing the ramp angle corresponds to increasing the adverse pressure gradient on the ramp surface). A closer look at Fig. 13a reveals that as one proceeds downstream in the vicinity of the surface, there is a rapid deceleration in the fluid velocity, which eventually leads to a region of reverse flow. This reverse flow zone which corresponds to dark blue velocity contours, starting at around X/H=1.7 and extending up to X/H=3.1 (H = 2.25″), indicates that a separation bubble with recirculating flow is visibly present. In physical dimensions, the separation region

for this case is ~3.2″, which is considerably larger than the case where the ramp is at lower angles, e.g. for 0° case, the recirculation bubble is only ~1.9″. This of course is expected, since higher ramp angles results in more adverse pressure gradients hence larger separation regions. A sample case of the velocity field at 65m/s, with a ramp angle of 5°, is also shown in Fig. 14. A comparison with the 40 m/s case of Fig. 13 confirms that the recirculation bubble is significantly larger, both in extent and magnitude.

To summarize, the adverse pressure gradient generated due to ramp geometry leads to a local separation of the incoming boundary layer, where the size of the bubble increases with the freestream velocity and ramp angle (adverse pressure gradient). Next we examine the effect of microjet control, especially its efficacy in controlling separation as the size of the separation region increases.

6.1.2 Effect of Microjet Control

When microjets at the appropriate locations were activated, the reverse/separated flow region is eliminated, with very low mass flux. This is demonstrate in the velocity contour plot shown in Fig. 13b where the microjet array at MJ4, at an angle of 90° relative to the local surface, has been activated at a stagnation pressure of 10psig. This effect of microjets was observed for all the conditions where the separated flow was present for the baseline case. A comparison with the baseline case in Fig. 13a indicates that, as was the case with the fixed ramp, the activation of microjets not only eliminated the reverse flow but the momentum near the surface increased significantly. Similar effects of control were observed at the highest velocity examined (65 m/s), where the extent and the magnitude of the separation region were much greater. This is seen in Fig. 14b, where microjet MJ5 at an angle of 90° to the ramp surface has been activated at 25psig and separation is completely eliminated. This effect of microjet control and the optimization procedure, i.e. identifying parameters to formulate a control strategy which has a maximal impact with minimal effort is discussed in subsequent sections.

In addition to simply characterizing the effect of separation and its control on the unsteady surface flow, another important goal of this research was to identify properties that are relatively sensitive to the state of the flow above the surface. These may perhaps then be used as input 'sensors' for a closed-loop control approach. Since separation is characterized by an increase in the unsteadiness and as such pressure fluctuations on the surface, we next examine the unsteady surface pressure as a possible means for identifying flow separation.

6.2 Unsteady Pressure Measurements

High frequency response Endevco® (Model 8510B-1) pressure transducers with a range of 0-1psi were used to obtain the unsteady pressure data at selected locations. These sensors were placed such that they were located both upstream and downstream of separation location. The location of these transducers has been shown in Fig. 12a. A representative dynamic pressure spectra for one of the transducers (TR4), located inside the separation bubble, is presented in Fig. 15. Measurements shown in the Fig. 15 includes the spectra for flow with and without control at 0° and 5° angle of attack case at X/H=2.7.

6.2.1 Baseline Flow (No Control)

A comparison of the spectra shown as dashed lines – red and black - in Fig. 15 clearly indicates that for the baseline flow, the pressure fluctuations increase dramatically - by almost a factor of two in the overall P_{RMS} levels, as the ramp angle increases from 0° to 5°. This corresponds to a significant increase in the pressure fluctuations with the ramp angle of attack. This behavior is also reflected in the PIV data; where changing the angle of attack increased the magnitude of mean reverse flow velocity and the size of the separation bubble, as seen in Figs. 13 and 14. This is concomitant with a substantial increase in the velocity fluctuations, V_{RMS}, in the separated region with increasingly large separations. This suggests that the unsteady pressure distribution, either alone or coupled with the mean pressures, may be used as a measure of the separation location and its size. This issue is addressed in more detail in subsequent sections.

6.2.2 Effect of Microjet Control

The unsteady pressures with the microjets activated are also presented in Fig. 15 as solid lines. It is evident that the activation of microjets results in a significant reduction in the pressure fluctuations for both the 0° and 5° case. For the cases shown here, the microjets are operating at a stagnation pressure of 25psig at an angle of 90° relative to the local surface. For both 0° and 5° cases the pressures fluctuations have been reduced by more than a factor of 2. This clearly illustrates the beneficial effects of the present flow control strategy, while again pointing to the use of the unsteady surface pressures as a possible input sensor for adaptive control strategies. To summarize, microjets were very effective in controlling separation and attaching the flow field globally. This phenomenon is also reflected in the unsteady pressure distribution over the surface. In the proceeding sections we describe the results of parametric experimental studies

through which we systematically explore the effect of microjet control parameters on properties such as the velocity and the pressure field.

6.3 Effect of Microjet Parameters

6.3.1 Effect of Microjet Location

It is generally believed that actuation closer to the separation location would produce the most beneficial results. Using the velocity field measurements, the separation location for a given flow conditions can be found and the effect of microjet actuator placement relative to this location can be examined. As discussed subsequently, the velocity field reveals that in general the microjets are most effective when activated upstream of the separation location. There also appears to be a range of locations upstream of separation, where their effect is optimal; once outside this range, either very close or too far upstream, the effect of control diminishes. However, for all the actuator locations examined to date, separation control could be achieved when the microjets were operated at the appropriate pressure. This required a systematic increase in the microjet pressure as one moves outside the optimal actuator placement zone.

Table 2 lists the locations for separation, actuators, and pressure transducers. A representative example of the velocity profiles for the 40 m/s case at a ramp angle of 5° is seen in Fig. 16, where U/U_{inf} is shown as a function of the vertical distance from the surface (Z/H) at a streamwise location of X/H=2.3. The location at which this data was extracted from the velocity field is shown as a dashed vertical white line on Fig. 14a. For control cases, the microjet angle relative to the surface is 68° and the microjet stagnation pressure is 10psig. As evident in Fig. 16a, different locations have a different effect on the velocity profile. Keeping in mind that for this case, the flow separates roughly at X/H~1.7, the activation of MJ2, which is significantly far upstream (at X/H ~ 0.7), at 10 psig does not lead to complete attachment; a very small reverse velocities can still be seen in the plot (MJ2: green curve). In contrast, the flow is completely attached with the activation of MJ5 (orange curve) located at X/H~ 1.3, i.e. much closer but still upstream of separation. Along the same lines, when MJ7 (@ X/H ~ 1.9, located *downstream* of the separation location, is activated the velocity profile deteriorates slightly relative to MJ5.

The corresponding unsteady pressure distribution at X/H=2.7, shown in Fig 17a, reveals similar results with higher overall P_{RMS} values for MJ2. As was the case for the mean velocity profiles of Fig. 16a, the P_{RMS} distributions of MJ5 and MJ7 are very similar, primarily, because the flow is attached for both cases. Partial flow attachment for MJ2 at these conditions, however, does not imply that the flow cannot be attached. For example, using MJ2, separation could be

completely eliminated using either a different microjet angle or a higher pressure. A sample result at the same location, obtained from the PIV data with a different microjet angle is shown in Fig. 16b°. With the same microjet pressure (10 psig), the flow is now attached when the MJ2 array is used. Our results show that when using 90° microjets, flow attachment is achieved for all actuator locations, MJ2 through MJ7.

Similar effects can be seen from the corresponding unsteady pressure spectra shown in Fig. 17b where the spectra for MJ2 at two angles. As seen here, there is a significantly larger reduction in the overall P_{RMS} values at 90° relative to 68°. Given that the flow was partially separated for 68° and attached for 90°, these results further substantiate the fact that a significant reduction in P_{RMS} is an indication of the flow attachment, complete or partial. What P_{RMS} values or range of values, indicate complete attachment needs to be explored and is commented on later. What the above results suggest is the significant potential of using the unsteady pressure signature to identify the flow state. A similar response, although not as dramatic, can also be observed by increasing the microjet pressure. This is seen in Fig. 16c where the microjet pressure is varied while keeping all other parameters the same. The flow is attached at a pressure of 15psig and the velocity profile continues to become 'fuller', indicating increased momentum near the surface, as the microjet pressure is increased. The unsteady pressure distribution for this case is shown in Fig. 17c. Similar behavior is seen with respect to the P_{RMS} values, which decreases with increasing actuator pressure. However, Figs. 16c and 17c also indicate that successive increments in the microjet pressures yield increasingly lower returns in terms of additional momentum in the boundary layer, i.e. fuller profiles, and lower P_{RMS} values.

The preceding results demonstrate that even for the worst control case scenario where the actuators are far upstream of the separation location, microjets reattach the flow completely – if sufficient supply pressures are used. Furthermore, the unsteady pressure signature directly reflects the response of the flowfield to control. Next we examine other control parameters specifically, microjet angle and microjet pressure. Both of these appear to have a significant impact on the flow properties and control efficacy as illustrated by the results just discussed.

6.3.2 Effect of Microjet Angle

The microjet angle is the angle relative to the local surface through which the flow is injected. Four different angles were studied within the constraints of our present set-up. The effect of microjet angle was primarily examined at two locations, MJ4 and MJ5. Representative velocity profiles at X/H=2.3, with microjets activated at MJ4 and MJ5 are shown in Fig. 18

where the microjets are operating at a constant pressure of 10psig for all the cases shown in Fig. 18. In Fig. 18a, the microjet array MJ4 has been activated; where based on the fullness of the profiles, these profiles suggest that best control is achieved at an injection angle of 75°. One also observes that the 68° injection angle produces a profile that is not as full as the 90° case. This suggests that there is an optimum angle to achieve the best results. It should be mentioned here that 68° doesn't mean that the microjets are blowing opposite to the freestream. Rather, due to the ramp geometry, the jets are actually blowing at an angle of 3° with respect to and into the direction of freestream.

To further investigate the coupling, if any, between the optimum angle and location, similar experiments were performed using the MJ5 array. These results are shown for X/H=2.3 in Fig. 18b which make it apparent that the optimal angle is no longer 75°. In fact, there is very little difference in the profiles in the near –wall region, between the 68°, 75° and 90° injection angles. This is indicative of the complex flow behavior and the strong interdependence between the various control parameters. It also suggests the need for other metric(s) that captures the effect of more than one parameter. Nevertheless, even though we are still attempting to understand the nuances of the various parametric effects to further optimize the use of microjets, it is very encouraging to see that this very simple approach is rather robust and yields significant benefits over a wide range of conditions with minimal cost and almost no associated penalties.

The unsteady pressure distributions shown in Fig. 19 further confirm the trends observed in the velocity profiles shown in Fig. 18. In the case of MJ4 (Fig. 19a), 75° and 105° arrays appear to be performing better. However, the difference in the spectra and the overall values for these cases is not very significant, probably because flow is attached for all the control cases.

6.3.3 Effect of Microjet Pressure

As mentioned earlier, and as evident from the results presented so far, microjet pressure is also a significant parameter. As seen in Fig. 16, at certain locations higher microjet pressure is required to control the flow. With this in mind, we investigated the pressure variation at the 'optimized control location', i.e. the location which required the least amount of momentum influx for control, MJ5. The microjet supply pressure was varied from 2 to 20 psig in increments of 2 psig and the microjet angle was fixed at 90°. Representative vertical velocity profiles from this experiment are shown in Fig. 20a for X/H =2.3. As seen from Fig. 20a, the separation was well controlled at 6 psig and saturation was observed beyond this pressure. This variation in the control effect is also seen in the unsteady pressure measurements shown in Fig. 20b. The spectra

shown in Fig. 20b reveal that overall P_{RMS} values decreases as the microjet pressure is increased, but after 10psig, the microjet effect is saturated (see Kumar *et al*[36]., for more details).

With the proper use of other control variables, this mass flow requirement is expected to go down further. The question is "how much lower?" OR "What should be the criterion for control?" Should the criterion just be that the flow is incipiently attached everywhere or should the increase in the momentum in the near-wall region of the boundary layer, i.e. the fullness of the boundary layer profile, be also considered? The answer to this question will likely come from a detailed cost function analysis, which is beyond the scope of this present investigation. What the present results show however is that the microjet pressure needed for the flow to be incipiently attached is ~5psig. When extrapolated to a theoretical inlet duct, e.g. a 30% boundary layer ingesting duct – a nominal value used for BWB inlet, this results in a mass flow requirement that is well below the maximum permissible bleed flow values as quoted by engine manufacturers. This suggests that engine bleed flow may be used to supply the gas for the microjet actuators.

6.4. Physical Mechanisms

Realizing that the microjets are very effective in the control of flow separation, the next issue that we investigate is the flow physics behind this effect. What effect(s) do the microjets have on the separated flow which is causing the flow to re-attach? Is it just the addition of high-energy fluid in the low-energy boundary layer or is it something more? The direct addition of momentum has already been ruled out as presented in our earlier calculations (§4). Traditionally, among the methods that have worked, flow attachment was achieved by the direct addition of momentum, removal of low momentum fluid from boundary layer or by the use of vortex-generators, which create streamwise vorticity and thus energize the boundary indirectly (see discussion in §1)[14,15,22,23]. As discussed earlier in §4, it is anticipated that the microjets are acting as "fluidic micro v.g.'s", which have been known to control the flow separation where they do so by generating streamwise vortices.

To investigate this anticipated mechanism and obtain quantitative measurements of the three-dimensional flow field, stereoscopic 3-component PIV measurements were made in the transverse planes at selected locations. In addition, these measurements allowed us to examine whether the initial separation was two or three-dimensional and if it was eliminated over the entire span of the model. These questions are critical if one is to apply this technique to complex three-dimensional geometries. Obtaining reliable two-component PIV measurements over large

regions is a challenging task in itself. Doing so using 3-component PIV increases the level of difficulty significantly. The only way to obtain all 3 velocity components was to view the flowfield from the front. However, since the ramp is inclined, the ramp surface reflects light from the laser sheet, thus decreasing the contrast and the quality of the PIV images. These reflections from the ramp surface made 3D-PIV measurements very difficult to obtain and required us to experiment with various seeding methods, ramp surface finish, optical arrangements and camera angles. As a result, the 3-component PIV measurements shown here required almost 8 months to complete.

6.4.1 Baseline Case

The locations where the 3-D PIV measurements discussed herein were obtained are indicated in Fig. 14 by dashed lines. An ensemble average of the flow-field at X/H = 2.3 is shown in Fig. 21a. The flow is symmetric, but somewhat shifted to the right side of the ramp, a behavior consistent with the surface flow visualization results presented earlier. This may be due to the fact that the geometric centre of the ramp does not exactly match the geometric center of the test section and is offset to the left by roughly the same distance. The presence of the separated flowfield can be clearly seen by the blue contours indicating a significant region of reverse flow roughly spanning the 40% of the ramp width. To provide a better representation of the velocity field, an isometric view of the flow field is shown in Fig 22a, where the velocity vectors in the reverse flow region have been superimposed on the contours. One can see that close to the surface, there is a zone of significant reverse velocity (indicated by the red arrows) and that the flow is highly 3-dimensional.

6.4.2 Effect of Microjet Control

When the microjets are activated, complete reattachment was achieved. Fig. 21b shows the effect of MJ5 operating at 25psig using 90° microjets. As seen in Fig. 21b and in Fig. 22b, flow is completely attached, where the blue contours, signifying reverse flow, have disappeared and the velocity vectors (indicated by red arrows) are now in the freestream direction. In addition to attachment, microjet control has also significantly energized the boundary wall fluid by transporting momentum from the outer layer of the boundary layer to the buffer layer. We believe that this mixing between the low momentum boundary layer fluid near the wall and the high momentum outer layer fluid is caused by streamwise vortices generated by microjets, which in turn is responsible for complete attachment of the separated flow.

To examine the flow physics further, measurements were obtained at planes very close to the activated microjets where our aim was to obtain direct evidence of the generation of streamwise vorticity due to their activation. Before continuing, it is worth reminding that the microjets are only 0.4mm in diameter and their direct penetration depth is less than the boundary layer thickness and for the most part it is confined to the buffer layer and regions below. As a first step, a transverse plane, 10 microjet diameters downstream of the microjets was selected for these measurements. At this distance, it was anticipated that the microjet 'plume' would have developed significantly such that its effects – e.g. the counter-rotating vortex pair[37]- will be more noticeable. Fig. 23a shows the velocity field and Fig. 23b shows the vorticity field for the baseline case. The contour plots have been shown only up to a height of 20mm above the surface to provide a higher resolution in these figures.(Note that the data very close to surface, up to 2-3mms, may be contaminated due to reflections from the surface.) The effect of control can be easily seen in upon comparing the flow with control, shown in Fig. 24, with the baseline case of Fig. 23. Note that at this streamwise plane, the flow without control is attached, as seen in Fig. 23a. When the microjets are activated, the green contours have shifted downwards which indicates mixing between the buffer layer (marked by green contour) and the outer layer (marked by red contour). This suggests that the some of the higher momentum in the outer layer has been transported to the buffer layer, which is closer to the wall. A closer examination of Fig. 24a suggests that traces of the microjet plume can be seen in the contours roughly 9mm above the surface. To confirm whether this is the location of the microjet plume centerline, we compare our data to the results obtained by Pratte and Baines[38,39] for jets in cross-flow. The *rd* length scale, as has been used by Pratte and Baines[38] was used to find the centerline trajectories of jet, using the correlation

$$\frac{y}{rd} = A\left(\frac{x}{rd}\right)^{m}$$

where A & m are constants, d is the jet diameter and r is jet to cross-flow velocity ratio. Using A=2.05 and m=0.28 for r=5 to r=35, the vertical displacement of the microjet in our case corresponds to y ~ 8mm. Assuming that the above scaling appliers here and accounting for the slope of the ramp, one would expect the microjet centerline to be roughly around 9mm.

With jet centerline thus located, we next examine the vorticity field in Fig. 24b. For clarity, we have marked the position of jet plume, as obtained using Pratte and Baines' correlation, by solid circles - the center being the location of microjet. One observes the presence

of significant streamwise vorticity around these solid circles. These high-vorticity areas have marked as dashed circles in Fig. 24b. It should also be pointed out that these vortices are of opposite sign and of almost equal strength. The generation of Counter-rotating Vortex Pairs (CVP's) due to jets in cross-flow is well-established and based on these measurements this mechanism appears to be at play in the current flow control approach. Fig. 24b also shows that the CVP's are slightly skewed with respect to the projected jet centerline. This might in part be due to the fact that there is an interaction between adjacent jets and that the flow is 3-dimensional.

A better visualization of the CVP's can be seen in Fig. 25 which shows a 'zoomed-in' view of a small section of the vorticity plot of Fig. 24b. In order to further enhance the effect of control, the baseline vorticity field has been subtracted from the vorticity contours shown here. The presence of significant streamwise vorticity in the form of CVPs is clearly visible. Also evident is the increased entrainment and missing due to these vortices as seen by the vectors superimposed on the contour plot in Fig. 25.

7. Concluding Remarks

The results presented in this report convincingly show the dramatic effect of microjets in controlling flow separation and distortion. Our results indicate that the effect of microjets varies with the amount of momentum supplied via the microjets (which is proportional to microjet pressure) and also with their location and angle at which momentum is injected. These parameters are coupled, sometimes strongly; however by choosing the appropriate combination of parameters separated flow could always be attached.

The detailed measurements reveal that the microjets energize the low momentum boundary layer flow by acting as fluidic vortex generators. The PIV measurements clearly indicate the presence of the counter-rotating streamwise vortices in the boundary layer which is the most likely mechanism behind the mixing within the boundary layer fluid. These vortices are known to promote the mixing of lower momentum boundary layer fluid with the outer higher momentum fluid and this enhanced mixing helps to control separation. The most significant advantage of using these actuators is that it can be optimized for the desired control effect, whether it is reattachment or separation reduction and/or distortion control. Furthermore, the jets can be activated/de-activated as needed, hence eliminating or drastically minimizing the increased drag as with the conventional vortex generators. Their effectiveness over the entire range of conditions examined to-date, combined with their simplicity; robustness and the minimal mass flow requirement make them attractive from a practical perspective.

The response of the flowfield to control inputs was also characterized in terms of on the unsteady pressure distribution. The unsteady pressure field was found to be directly responsive to the state of the flow above the surface, where separation reduction or elimination led to measurable reductions in the unsteady pressures. As such, the unsteady pressure signature appears to be a strong candidate for a 'flow state sensor' (indicating location and the magnitude of the separation). Once better understood and properly utilized, this behavior can be of significant practical importance for developing and implementing online control. We plan to continue our study and development of this approach for separation and distortion control, hopefully with external grant support. We also plan to implement at a minimum, a quasi closed-loop control strategy where unsteady pressure transducers are used as sensors for detecting separated flow which in turn will be used to determine the optimal microjet operating parameters. Through a much better understanding of these properties, we hope to devise an optimal microjet-based control scheme which can be adapted to more complex and realistic configurations.

8. References

1. MacMartin, D.G., Verma A., Murray R.M., Paduano J.D., "Active Control of Integrated Inlet/ Compression systems" FEDSM2001-18275, June 2001.

2. Mayer, D.W., Anderson, B.H., Johnson T.A., "3D Subsonic Diffuser Design and Analysis", AIAA Paper 98-3418.

3. Wellborn, S. R., Reichert, B.A., Okiishi, T.H., "Study of Compressible Flow in a Diffusing S-Duct", *Journal of Propulsion and Power*, Vol. 10, No. 5, Sept-Oct 1994, pp. 668-675.

4. Liebeck, R.H., "Design of Blended Wing Body Subsonic Transport", *Journal of Aircraft*, Vol. 41, No. 1, January-February 2004.

5. Rabe, D., Boles, A. and Russler, P. "Influence of Inlet Distortion on Transonic Compressor Blade Loading", AIAA Paper 95-2461.

6. Wygnanski, Seifert A., "Delay of Airfoil Stall by Periodic Excitation" *AIAA J Aircraft* 1996; Vol. 33(4):691–8.

7. Chang, P.K., "Control of Flow Separation", Hemisphere Publishing Corporation and McGraw Hill, New York, USA, 1970, pp. 154-177.

8. Gad-el-Hak M, Bushnell D.M., "Separation Control: A Review", *Journal of Fluids Engg.,* 1991; 113:5-30.

9. Schlichting H., "Aerodynamische Probleme des Höchstauftriebes" Z. Flugwiss. Bd. 13, 1-14.

10. Thomas F., "Untersuchungen über die Erhöhung des Auftriebes von Tragflügeln mittels Grenzschichtbeeinflussung durch Ausblasen" Z. Flugwiss., Bd. 10, 46-65.

11. Mokhtarian F., Modi V.J., "Fluid Dynamics of Airfoils with Moving Surface Boundary Layer Control," *Journal of Aircraft*, 1988, Vol. 25, pp.163-169.

12. Prandtl L. "Proceedings of Third International Mathematical Congress", Heidelberg, 1904, p. 484-91.

13. Betz A. "History of Boundary Layer Control", Germany. In: Lachmann GV, editor. Boundary Layer and Flow Control: Its Principles and Applications, Vol.1, New York: Pergamon Press, 1961. pp. 1-20.

14. Storms B. L, Ross JC. "Experimental Study of Lift-Enhancing Tabs on a Two-Element Airfoil." *AIAA J Aircraft* 1995; Vol. 32: 1072-8

15. Lin, John C. "Review of Research on Low Profile Vortex Generators to control Boundary Layer Separation", *Progress in Aerospace Sciences* Vol. 38(2002), p. 389-420.

16. Zaman K.B.M.Q., Bar Sever A, Mangalam S.M., "Effect of Acoustic Excitation on the flow over a Low-Re Airfoil", *Journal of Fluid Mechanics,* 1987,182:127-48.

17. Ahuja K.K., Whipkey R.R., Jones G.S., "Control of Turbulent Boundary Layer by Sound", AIAA Paper 83-0726, 1983.

18. Amitay M., Pitt D., Glezer A. "Separation control in duct flows", *Journal of Aircraft* Vol. 39, No. 4, July – August 2002.

19. Jenkins, L.N., Gorton, S.A., Anders S.G., "Flow Control Device Evaluation for an Internal Flow with an Adverse Pressure Gradient" AIAA Paper 2002-0266.

20. Greenblatt D., Wygnanski, I.J., "The Control of Flow Separation by Periodic Excitation", *Progress in Aerospace Sciences* Vol. 36(2000), p. 487-545.

21. Alvi, F. S., Elavarsan R., Shih, C., Garg G., and Krothapalli, A., "Control of Supersonic Impinging Jet Flows using Microjets," *AIAA Journal*, 2003 Vol. 41(7), p. 1347-1355.

22. Johnston J.P., Nishi M., "Vortex Generator Jets- Means for Flow Separation Control", *AIAA Journal*, 1990 Vol. 28, No. 6, pp.989-994.

23. Lou H., Alvi F.S., Shih C., "A PIV study of Supersonic Impinging Jet", AIAA Paper 2003-3263, 9th AIAA/CEAS Aeroacoustics Conference and Exhibit, May, Hilton Head, South Carolina.

24. Stratford, B.S., "The Prediction of Separation of Turbulent Boundary Layer", *J. Fluid Mech.* 5, 1-16, 1959b.

25. Kumar, V., Alvi, F.S. "Use of Supersonic Microjets for Active Separation Control in Diffusers", *AIAA Journal, Feb 2006*.

26. Kumar V., Alvi F.S. "Active control of Boundary Layer Separation & Flow distortion in Adverse Pressure Gradient Flows via Supersonic Microjet" NASA Report: NAG1-01057

27. Barberpoulos A.A, Garry K.P., "The Effect of Skewing on the Vorticity produced by an Air jet Vortex Generator", *The Aeronautical Journal*, March 1998.

28. Lourenco, L.M., "True Resolution PIV: A Mesh Free Second Order accurate Algorithm" International Conference in application of lasers in Fluid mechanics, Lisbon, Portugal, July 2000

29. Lourenco, L.M., Krothapalli A., "Mesh Free Second Order Algorithm for PIV Processing", Proceedings of the International conference on Optical technology and Image Processing in Fluid, Thermal and Combustion Flows, Yokohoma, Japan, Dec. 1998, pp. 24.

30. Norster E.R., "Jet penetration and mixing studies". Unpublished work, College of Aeronautics, Cranfield. See Reference 33.

31. Lefebvre, A.H., "Gas turbine combustion" McGraw Hill, New York, 1983.

32. Alvi, F.S., "The role of Streamwise Vorticity in the Control of Impinging Jets", FEDSM2003-45062.

33. Papamoschou D., Hubbard D.G., "Visual Observations of Supersonic Transverse Jets", *Experiments in Fluids* Vol. 14(1993), pp. 468-471.

34. Marzouk, Y. M., Ghoniem, A.F. "Mechanism of Streamwise Vorticity Formation in a Transverse Jet", AIAA Paper 2002-1063.

35. Marzouk, Y. M., Ghoniem, A.F. "Vorticity formulation for an actuated jet in crossflow", AIAA Paper 2004-0096.

36. Kumar, V., Alvi, F.S. "Efficient Control of Separation Using Microjets", AIAA Paper 2005-4879.

37. Fric, T. F. & Roshko, A., "Vortical structure in the wake of a transverse jet", *Journal of Fluid Mechanics,* 1994, Vol. 279, pp. 1-47.

38. Pratte, B. D. ,Baines, W. D., "Profiles of the round turbulent jet in a cross flow", *J. Hydronaut. Div.* ASCE 1967, Vol. 92, 53-64.

39. Smith S.H., Mungal M.G., "Mixing, structure and scaling of the jet in crossflow", *Journal of Fluid Mechanics,* 1998, Vol. 357, pp.83-122.

9. Students Supported

The following students were in part supported by this grant during their graduate studies:

1. V. Kumar - MS, 2003; presently pursuing a PhD (expected completion, Dec. 2006)

2. C. Davy – MS, 2003

3. O. Egungwu - MS, 2004

10. Publications Resulting from Research Supported by this Grant

1. Kumar, V. and Alvi, F. S*.,* "Use of High-Speed Microjets for Active Separation Control," *AIAA Journal,* vol. 44 , No. 2, Feb. 2006, pp. 273-281

2. Kumar, V. and Alvi, F. S., "Efficient Control of Separation using Microjets," AIAA Paper 2005- 4879, 35th AIAA Fluid Dynamics Conference and Exhibit, June 6-9, 2005, Toronto, Canada.

3. Kumar, V. and Alvi, F. S*.,* "Active Control Of Flow Separation Using Supersonic Microjets," ASME 2003 Fluids Engineering Meeting, July 6-10, 2003, Honolulu, Hawaii.

4. Kumar, V., Alvi, F.S. "Use of Supersonic Microjets for Active Separation Control in Diffusers", AIAA Paper 2003-4160.

5. Davy, C., Alvi, F. S. and Naughton, J. W. "Surface Flow Measurements of Micro-Supersonic Impinging Jets," AIAA Paper presented at the AIAA Ground Measurement Technology Conference, St. Louis, Missouri, 24 – 27, Jun 2002

6. Davy, C., Alvi, F. S and Naughton, J. W. "Flowfield and Surface Flow Measurements of Supersonic, Free and Impinging Microjets," The 10th International Symposium on Flow Visualization, August 26-29, 2002, Kyoto, Japan.

7. Phalnikar, K. A., Alvi, F. S. and Shih, C. "Behavior of Free and Impinging Supersonic Microjets," AIAA Paper 2001-3047

Table 1: Momentum injected versus Momentum gain achieved for various microjet pressures.

Microjet activated	Microjet Pressure	C_μ (%)	Momentum Gain Ratio (MGR)
MJ1	10	11.76	13.22
MJ1	15	19.58	9.53
MJ1	20	29.06	4.71
MJ1	25	39.71	7.44
MJ3	10	11.76	49.61
MJ3	15	19.58	40.38
MJ3	20	29.06	33.56
MJ3	25	39.71	28.78

Table 2: Ramp Configuration: Actuator and Separation Location

Ramp Height (H)	2.25″	
	Approximate Locations (X/H)	
	MJ2	0.7
	MJ3	0.9
Microjets	*MJ4*	1.0
	MJ5	1.3
	MJ6	1.5
	MJ7	1.9
Separation begins	40 m/s	1.7
Reattachment	40 m/s	3.1

Fig. 1- Ramp model, mounted in the wind tunnel
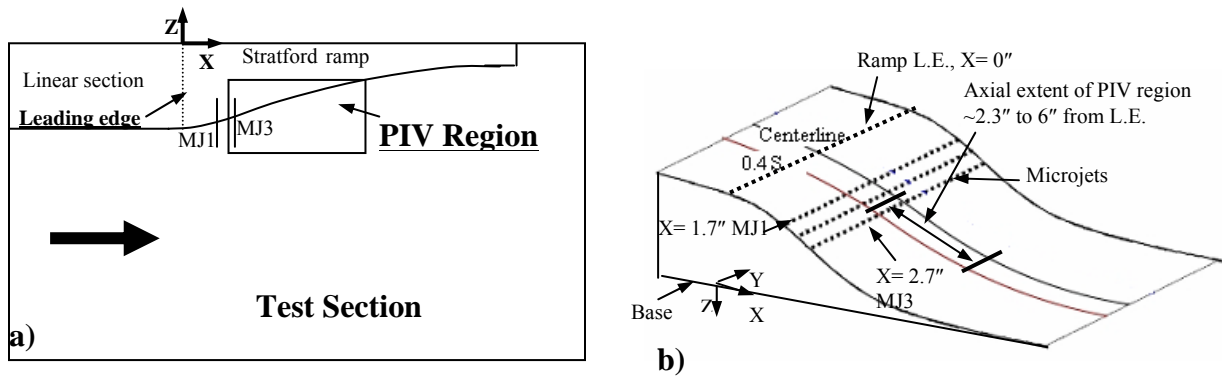
Fig. 2- **a)** Schematic of the test section

b) Detailed schematic of the ramp model
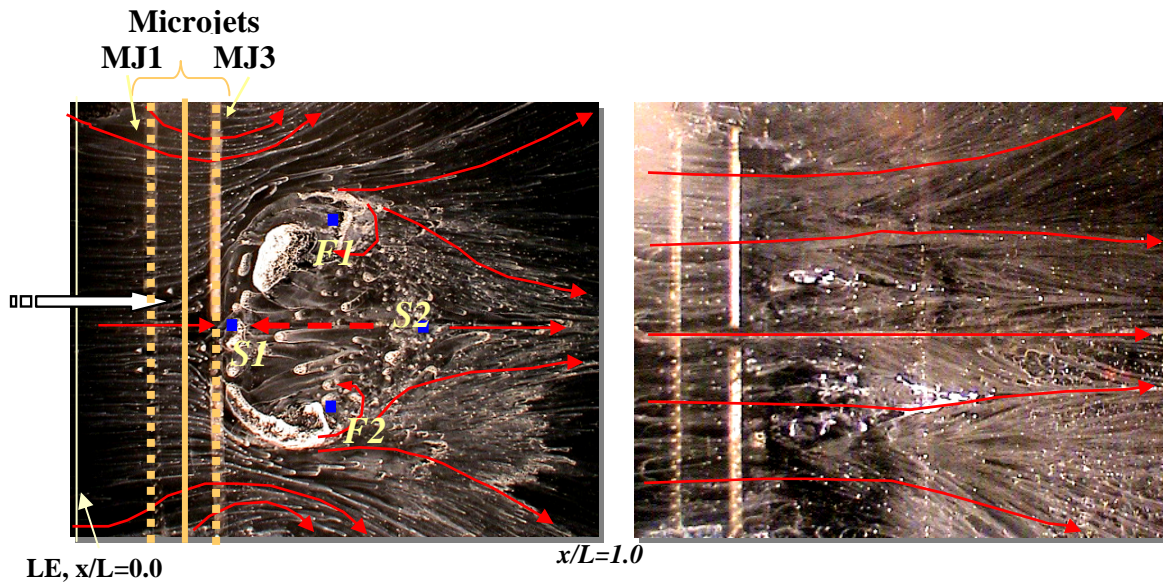
Fig. 3- Surface flow traces at 40m/s;

a) *No control* **b)** MJ3@25psig
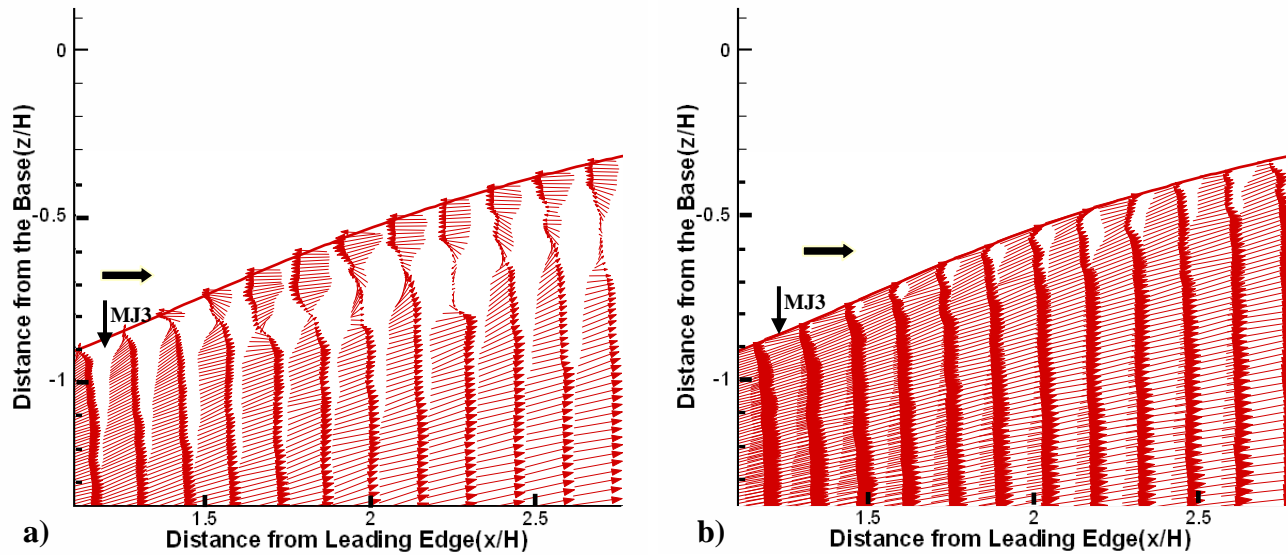
Fig. 4- **a)** Processed velocity vectors, *No Control* at 40m/s

b) Processed velocity vectors, *MJ3@25psig* at 40m/s
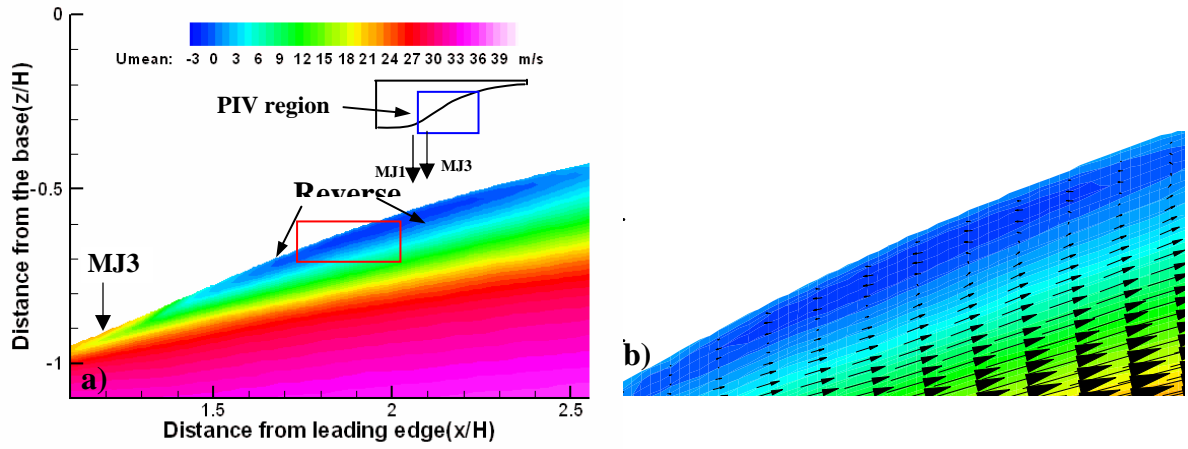
Fig. 5- Velocity field for 40m/s; *No Control.*

a) Streamwise velocity component, U **b)** Velocity vector for region indicated in (a)
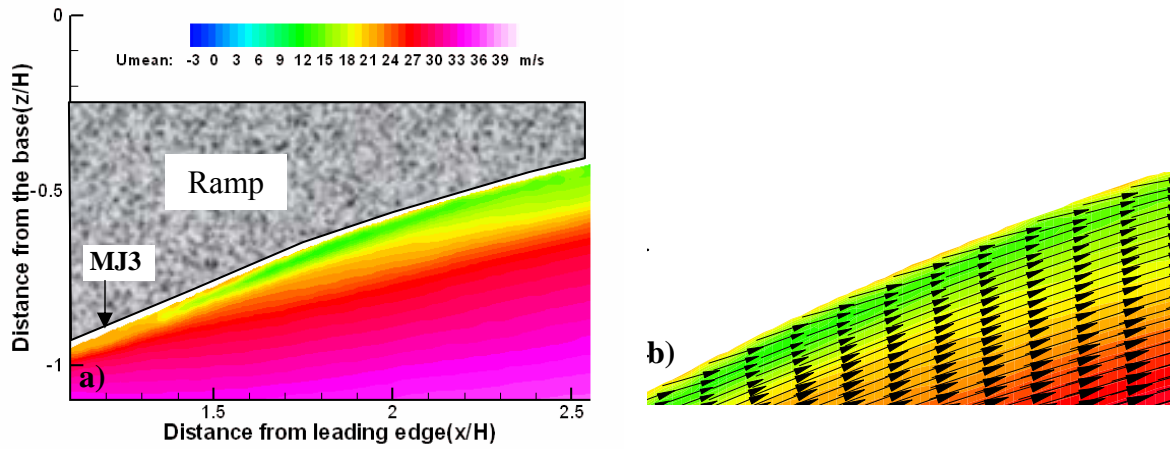
Fig. 6- Velocity field for 40m/s; *MJ3@25psig.*

a) Streamwise velocity component, U **b)** Velocity vector for region indicated in (a)
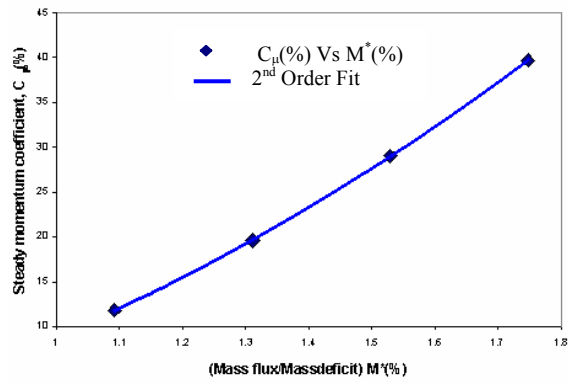
Fig. 7- Steady momentum coefficient, C_μ Vs. Mass flux coefficient, M^*
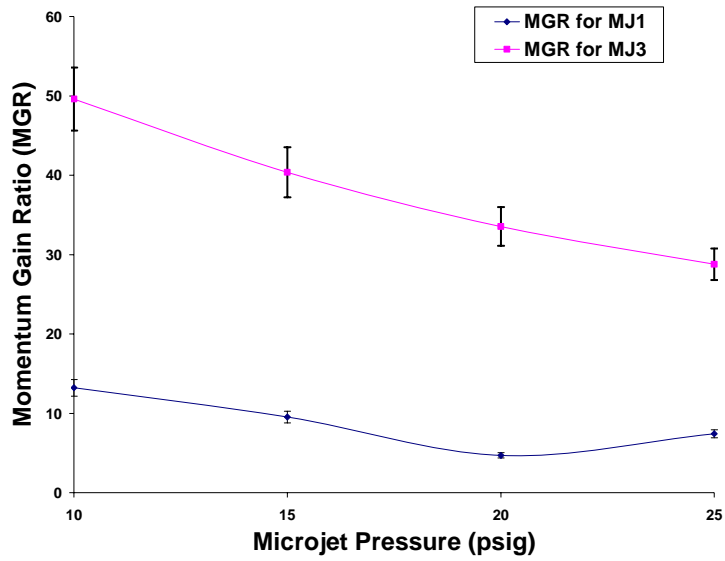
Fig. 8- Effect of Microjet location on MGR
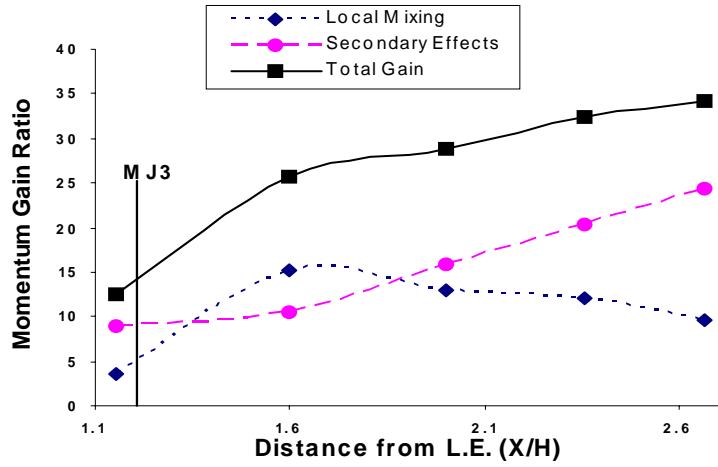
Fig. 9- A Comparative look at Microjet effects; MJ3@25psig
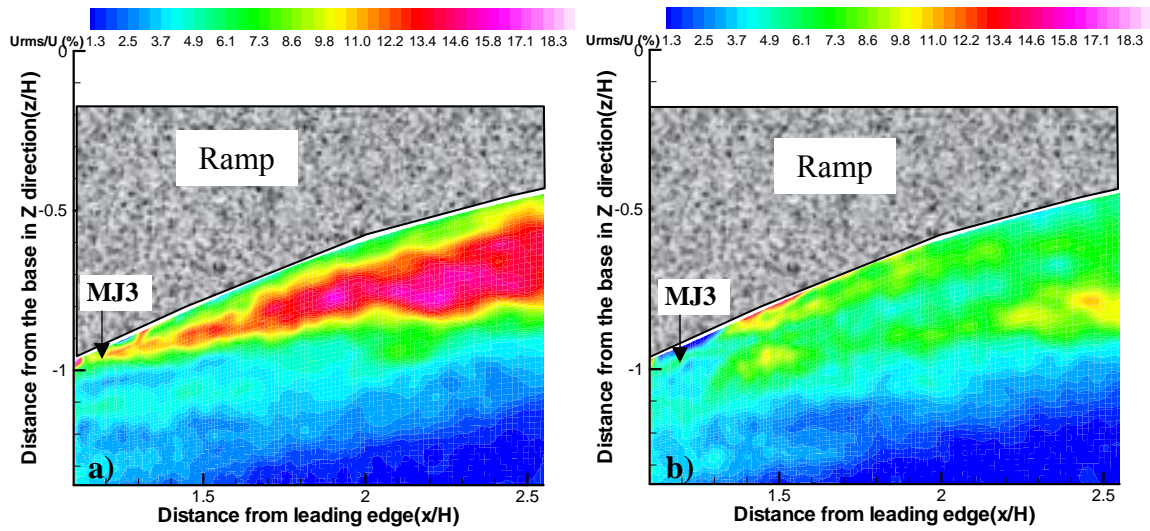
Fig. 10- Root mean square (U$_{rms}$) velocity;

a) *No Control* **b)** *MJ3@25psig*
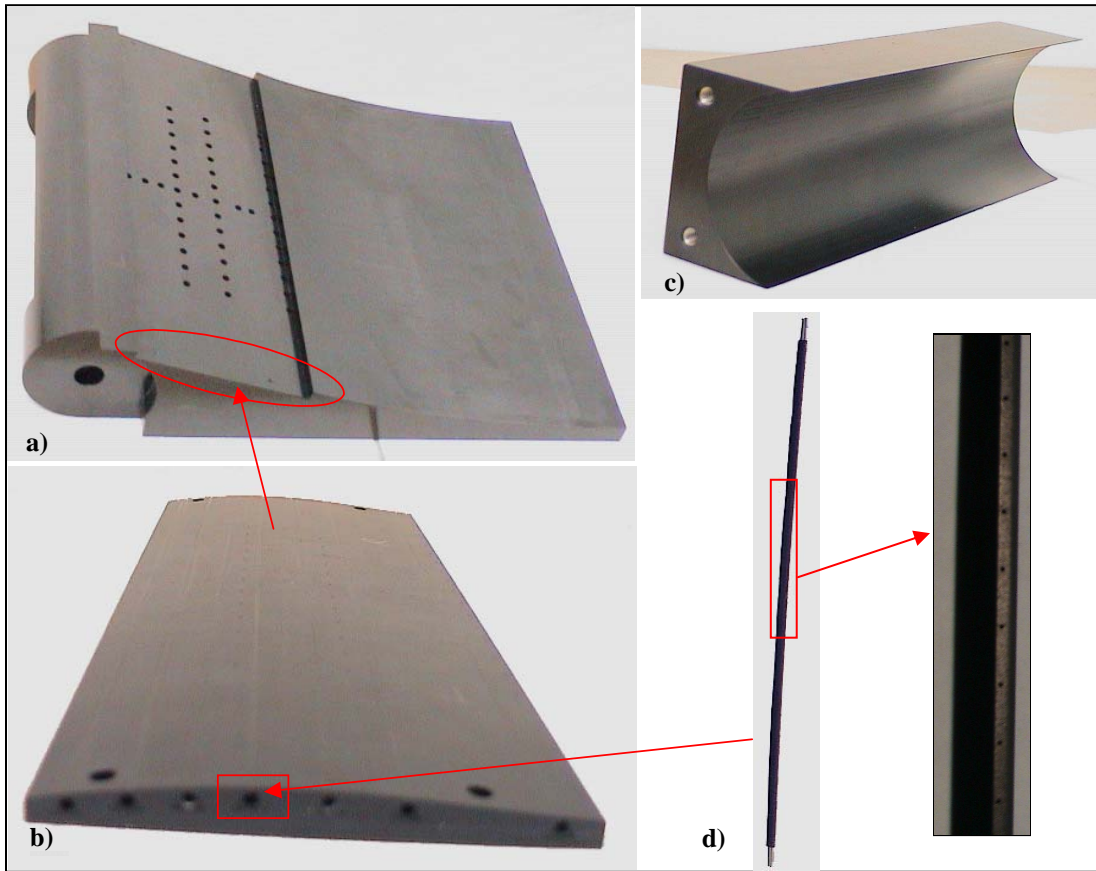
Fig. 11- a) New ramp model **b)** Microjet actuator insert which slides into the ramp model **c)** Hinge, to which the ramp attaches; allows for changes in ramp angle. **d)** Microjet array inserts which slide into the insert shown in b).
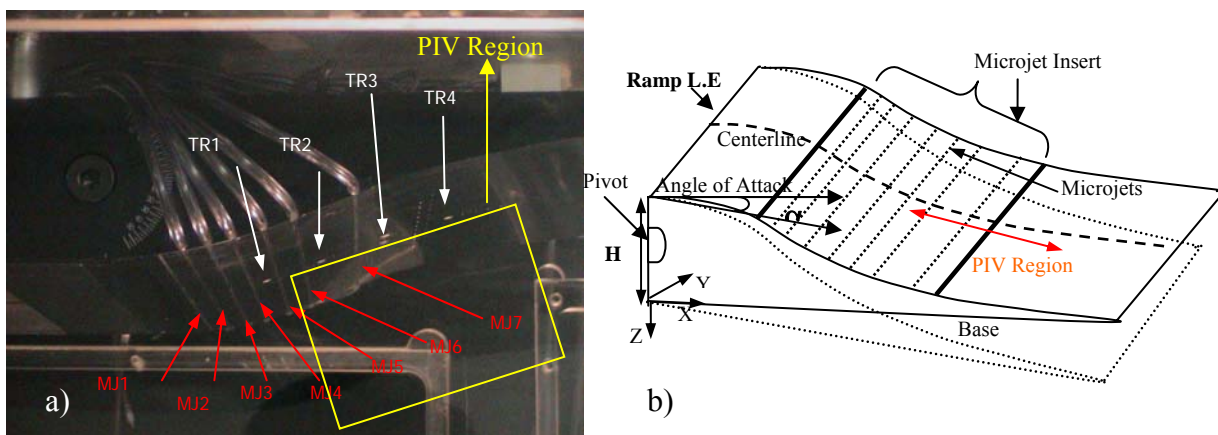
Fig. 12- a) Test model mounted in the test section
b) Schematic of the test model
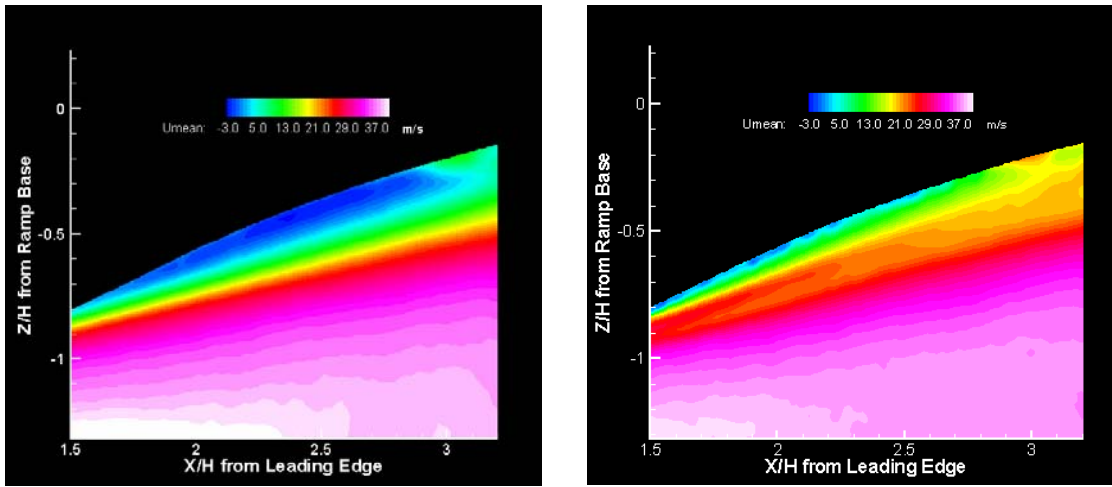
Fig. 13- a) Streamwise velocity data @40m/s: No Control

b) Streamwise velocity data @40m/s: MJ4; 90°; 10psig
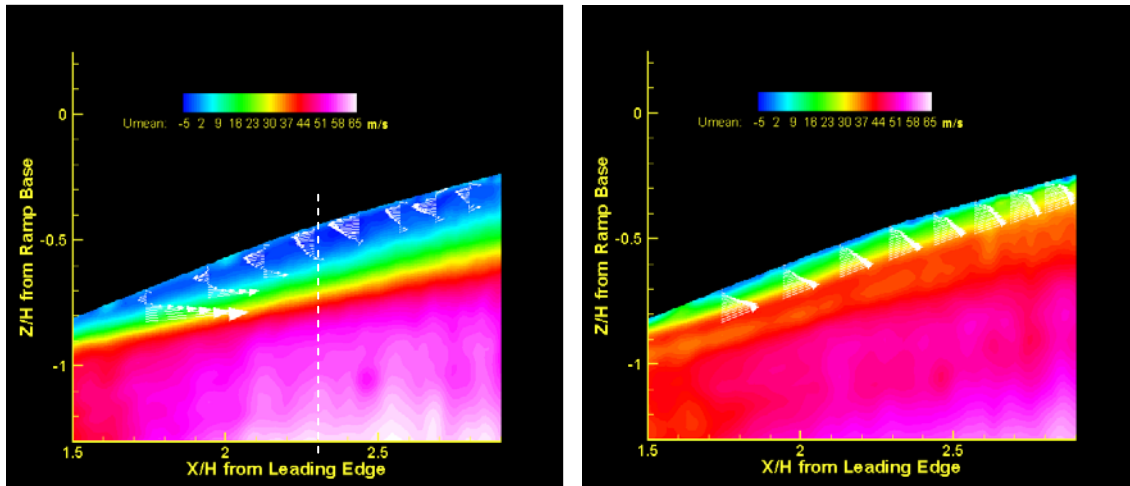
Fig. 14- a) Streamwise velocity data @65m/s: No Control

b) Streamwise velocity data @65m/s: MJ4; 90°; 10psig
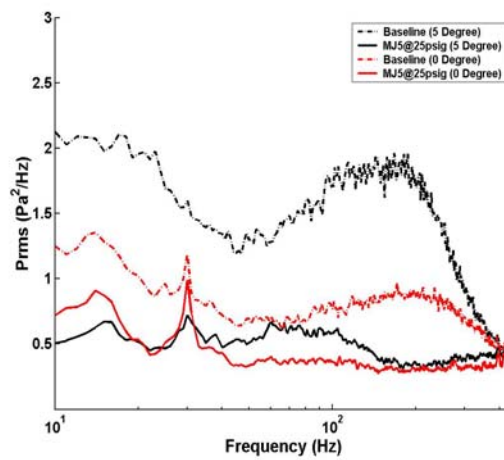
Fig. 15- Unsteady Pressure Spectra for U_∞= 40 m/s
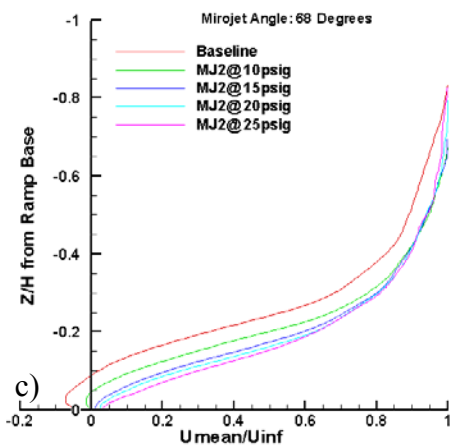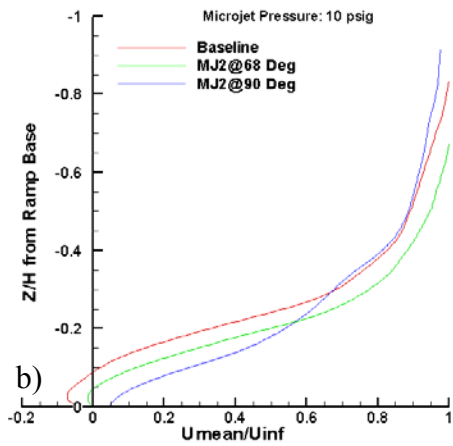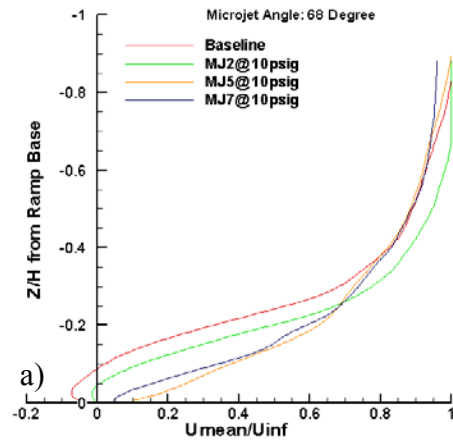
Fig.16- Effect of Parametric variation (Location, Angle, Pressure) on mean velocity profiles X/H=2.3, U = 40 m/s, Ramp angle = 5°
a) MJ2, MJ5, MJ7; 68°; 10psig
b) MJ2; 68°, 90°; 10psig
c) MJ2; 68°; 10, 15, 20, 25psig
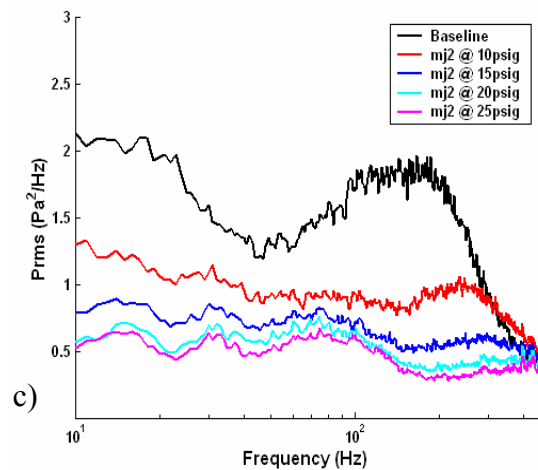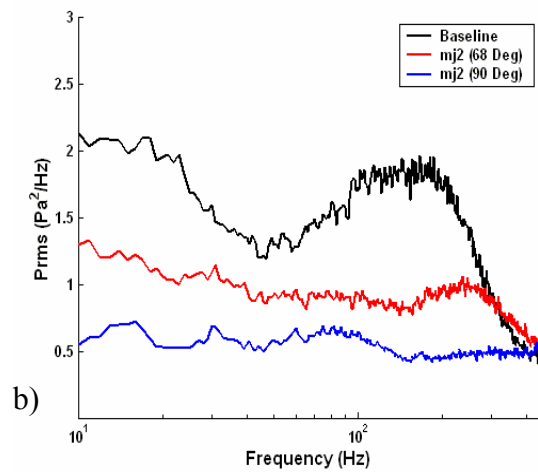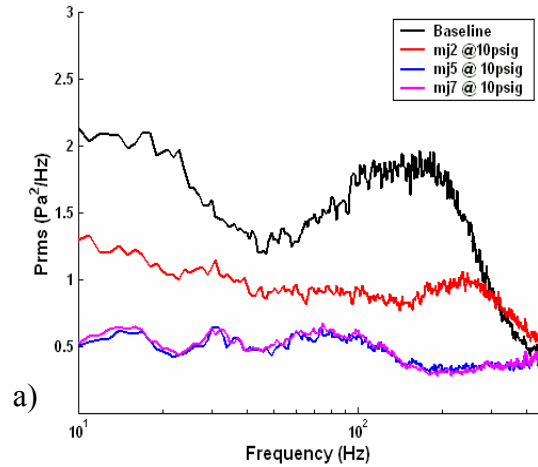
Fig.17- Effect of Parametric variation (Location, Angle, Pressure) on Unsteady pressure spectra at X/H=2.7, U = 40 m/s, Ramp angle = 5°
a) MJ2, MJ5, MJ7; 68°; 10psig
b) MJ2; 68°, 90°; 10psig
c) MJ2; 68°; 10, 15, 20, 25psig
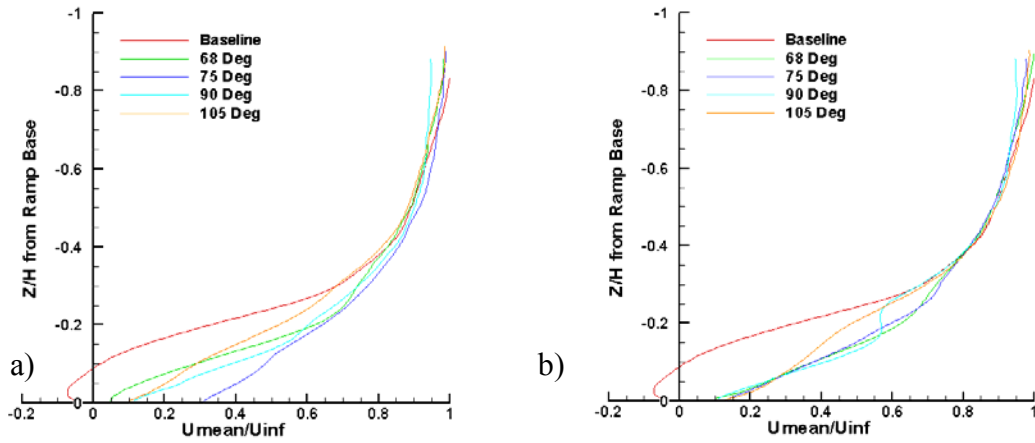
Fig. 18- The Effect of Parametric variation (Angle) on mean velocity profiles X/H=2.3, U = 40 m/s, Ramp angle = 5°; a) MJ4; 10psig b) MJ5; 10psig
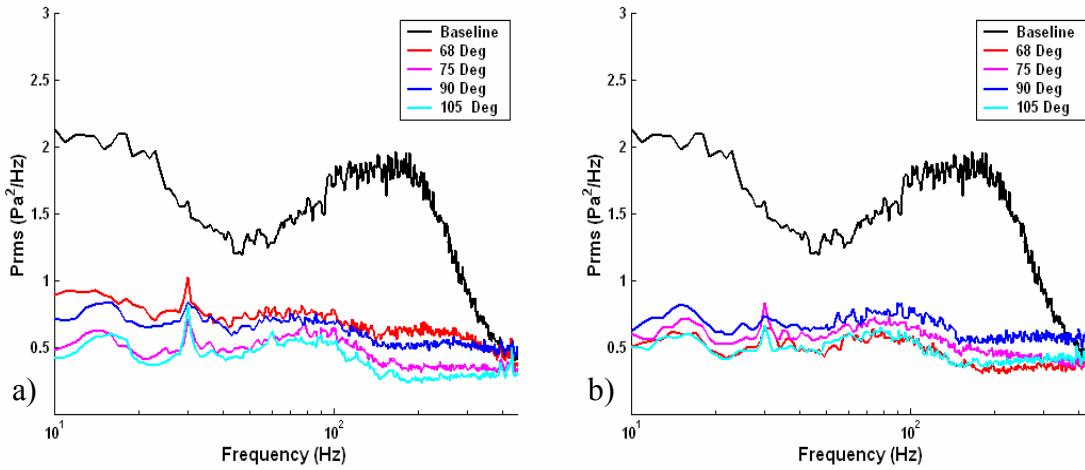
Fig. 19- Effect of Parametric variation (Angle) on Unsteady surface pressure X/H=2.7, U = 40 m/s, Ramp angle = 5°
a) MJ4; 10psig b) MJ5; 10psig
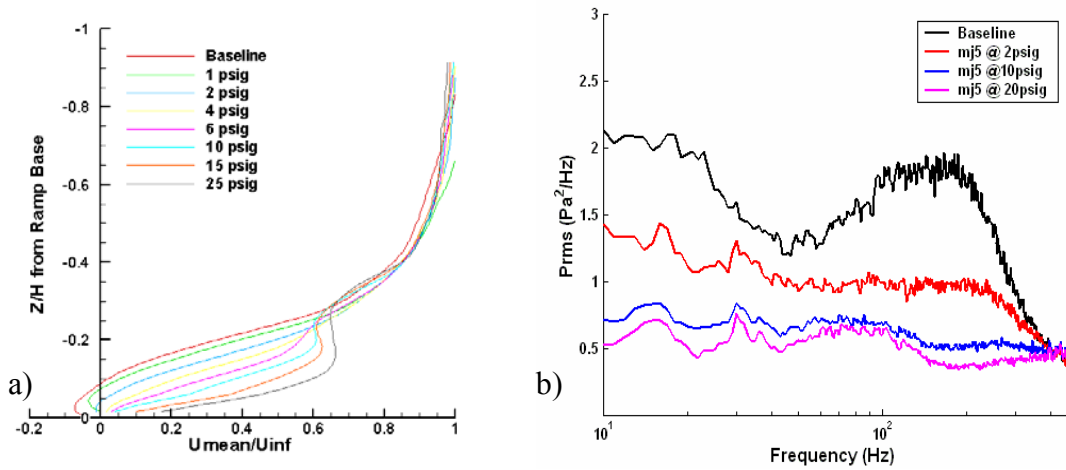
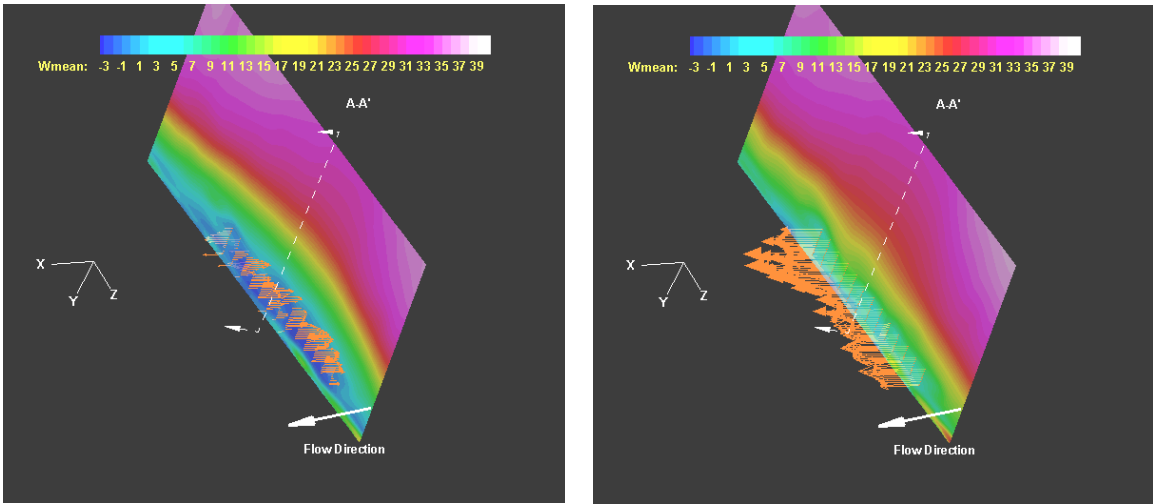**Fig. 20-** Effect of Pressure Variation (for U=40m/s, Ramp angle=5°)
a) on mean Velocity profile at X/H=2.3;MJ5;90°;0,1,2,4,6,10,15,25psig
b) on Unsteady surface pressure at X/H=2.7; MJ5; 90°;0,2,10,20psig
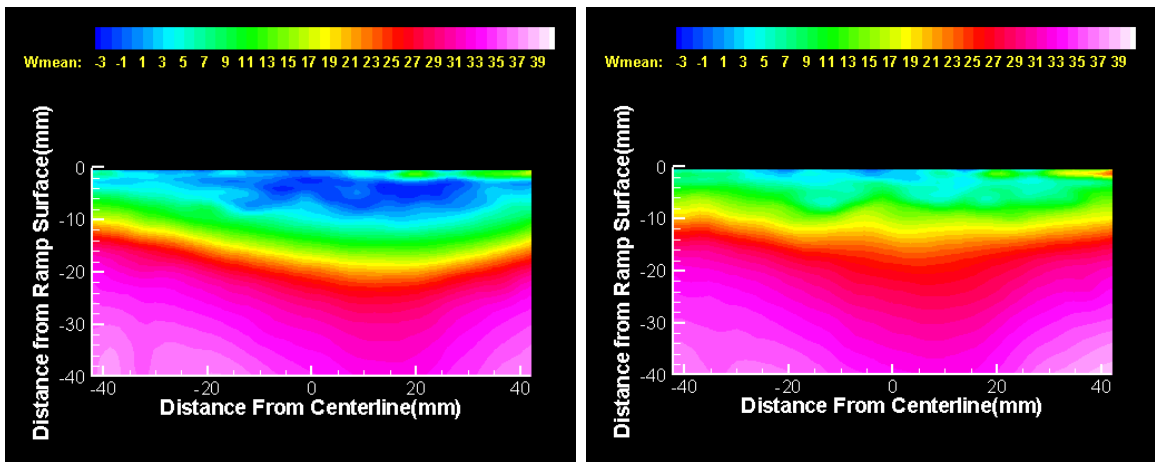
Fig. 21- a) 3D-Velocity data @40m/s; X/H =2.3; No Control
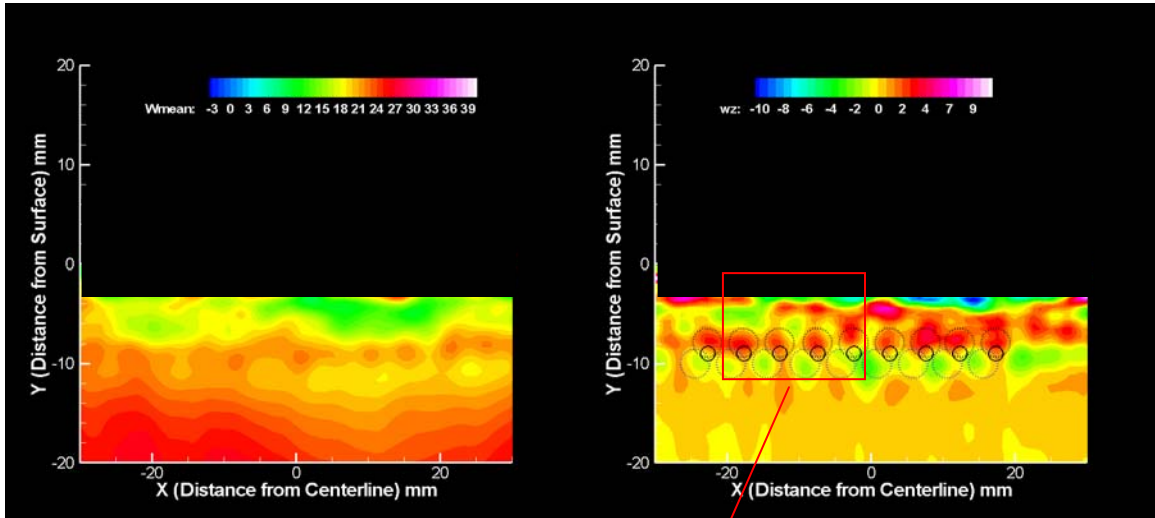
b) 3D-Velocity data @40m/s; X/H =2.3; MJ5; 90°; 10psig

Fig. 22- a) Isometric view showing the velocity vectors; X/H =2.3; No Control

b) Isometric view showing the velocity vectors; X/H =2.3; MJ5; 90°; 10psig
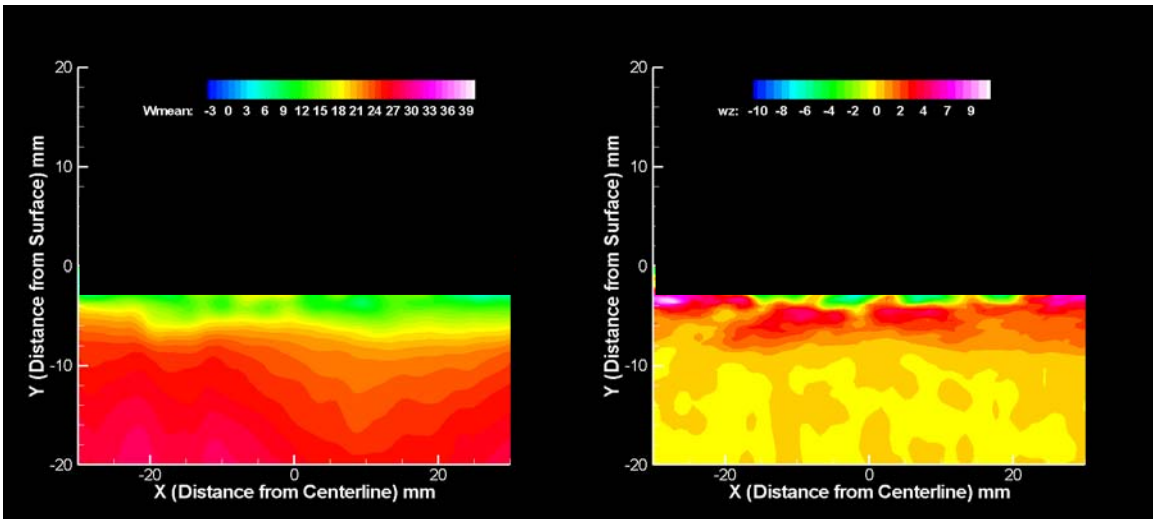
Fig. 23- a) Velocity Field 10 jet diameters downstream; *No Control*

b) Vorticity Field 10 jet diameters downstream; *No Control*

Fig. 24- a) Velocity Field 10 jet diameters downstream; MJ5@180slpm; 90°

b) Vorticity Field 10 jet diameters downstream; MJ5@180slpm; 90°
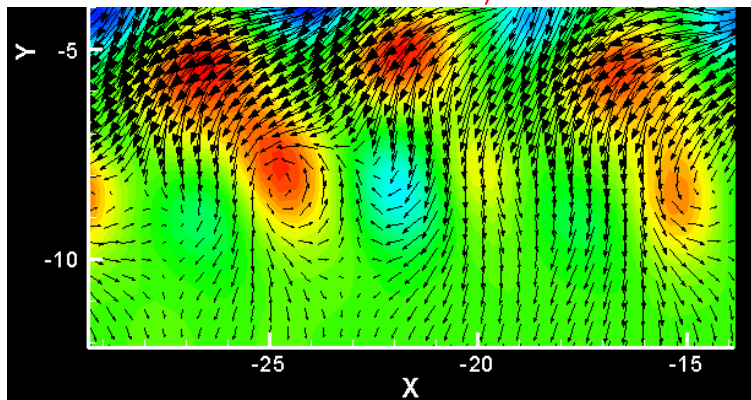
Fig. 25- A close-up of the vorticity field (in a subsection of the area in Fig.24b) showing the presence of counter-rotating, streamvise vortices.